Arab J Sci Eng (2014) 39:3199–3207
DOI 10.1007/s13369-013-0910-9

RESEARCH ARTICLE - MECHANICAL ENGINEERING

Springback Predictions of a Dual-phase Steel Considering Elasticity Evolution in Stamping Process

Murat Ozsoy · Emre Esener · Suphan Ercan · Mehmet Firat

Received: 2 May 2012 / Accepted: 15 November 2012 / Published online: 21 November 2013

Abstract Mechanical properties of a dual-phase steel of 0.8 mm thickness are investigated with uniaxial tensile loadings at room temperature. Standard tensile tests are conducted to determine Young's modulus, flow curves and plastic strain ratios in rolling, transverse and diagonal directions, respectively. Moreover, uniaxial tensile loadings with unloading–reloading cycles are performed to determine the elastic modulus evolution. Anisotropy of DP600 steel is described using isotopic hardening plasticity in junction with Hill's orthotropic yield function and applied in finite element (FE) stamping analysis of an automotive structural member. In sheet metal deformation modeling, material models with both constant and variable Young's moduli were considered to assess the effect of stiffness degradation on FE springback predictions. Effective plastic strain and part thickness distributions calculated with both models were fairly similar and maximum differences were determined to be 4 and 6 %, respectively. A similar situation holds for predicted springback distributions, but springback magnitudes calculated with variable modulus model were constantly higher. Computed geometries with both FE models were, furthermore, evaluated with surface scanning of manufactured parts. While stamping geometries predicted with both models underestimate actual shape distortions determined in manufactured parts, calculations with variable modulus have reduced maximum geometric deviation by 20 % and constantly improved shape correlation.

M. Ozsoy · S. Ercan · M. Firat (✉)
Department of Mechanical Engineering, University of Sakarya, 54187 Sakarya, Turkey
e-mail: firat@sakarya.edu.tr

E. Esener
Department of Mechanical Engineering, Bilecik University, Bilecik, Turkey

Keywords Ferrous metals and alloys · Stamping · Plasticity · Springback analysis

الخلاصة

تم التحقيق في الخواص الميكانيكية لحديد صلب ثنائي الطور (DP) من 0.8 مم سماكة مع أحمال شد أحادية المحور في درجة حرارة الغرفة. وأجريت اختبارات الشد القياسية لتحديد معامل يونغ، منحنيات التدفق ونسب سلالة البلاستيك في اتجاهات اللف، العرضية والقطرية على التوالي. وعلاوة على ذلك، تم تنفيذ أحمال الشد أحادية المحور مع دورات تفريغ - تحميل لتحديد تطور معامل المرونة. تم وصف تباين صلب DP600 باستخدام تصلب اللدونة النظائري مع تقاطع مع وظيفة عائد هيل متعامدة التغاير وتطبيقها في تحليل ختم العنصر المحدود (FE) لعضو هيكلة السيارات. وفي نمذجة تشوه الصفائح المعدنية، تم الأخذ في الاعتبار نماذج المواد مع كل من معاملات يونغز ثابتة ومتغيرة من أجل تقييم أثر تدهور الصلابة في تنبؤات تبريد وعمل FE. وكانت سلالة البلاستيك الفعالة وتوزيعات سمك القطعة المحسوبة من كلا النموذجين مماثلة إلى حد ما وتم تحديد الحد الأقصى للاختلافات ليكون 4 و 6 % على التوالي. وتم الحصول على حالة مماثلة لتوزيعات تنبؤات التبريد - العمل ، ولكن كانت مقادير تنبؤات التبريد - العمل المحسوبة مع نموذج معامل متغير هي أعلى باستمرار. وتم علاوة على ذلك تقييم الهندسات المحسوبة مع كلا نموذجي FE، مع مسح سطح الأجزاء المصنعة. في حين أن هندسات الختم المتنبأة من كلا النموذجين تقلل تشوهات الشكل الفعلي المحددة في الأجزاء المصنعة، فإن الحسابات مع معامل متغير قد قللت الانحراف الهندسي الأقصى بنسبة 20 % وحسنت بشكل مستمر باستمرار ارتباط الشكل.

1 Introduction

The demand on lower fuel-consumption as well as ever-reducing emission standards puts serious constraints on vehicle development programs in almost all automotive companies. Among other potential factors, today, the use of lightweight and high-strength materials is one of the ways of practically handling improved fuel-economy requirements in developing auto-bodies with efficient crash-energy

management [1]. Advanced high-strength steels (AHSS), in particular, provide a convenient means of reducing overall body weight while retaining essential structural stiffness and integrity of the vehicle. Therefore, in the last decade, conventional steel grades in many structural members have been replaced with their AHSS counterparts [2,3]. The increasing use of high-strength steels in sheet metal parts, however, brings about formability and shape distortion problems that can not be easily solved compared to stamping processes involved with conventional, highly formable steel grades [4]. The relatively high strength-to-elastic modulus ratio of AHSS is considered to be one of the main factors leading to difficulties to achieve a defect-free stamping part within desired dimensional tolerances [5].

Process design approaches based on FE simulation techniques have experienced similar difficulties with high-strength steel applications, and their effectiveness has been questioned particularly for springback predictions [6, 7]. This situation has led to new developments in element technologies, explicit–implicit solution algorithms and advanced plasticity models accounting Bauschinger effect and other complex deformation phenomena [8–11]. From presented experimental and FE studies, the influence of numerical parameters and modeling techniques has been well understood, and with the achieved developments in cyclic plasticity modeling, very accurate springback predictions were also obtained for various sheet metal geometries [12]. Today, various damage-coupled plasticity models exist for the quantitatively enhanced description of the sheet metal deformations and for an accurate calculation of springback [13]. But as model's capabilities improve, the number of material parameters necessary for the description of deformation process also increases. This essentially leads to more complex material testing and usually special mathematical techniques to determine these model parameters [14]. This may be an undesirable situation from an industrial perspective, since the simple tension test is usually the only available material data during tooling design phase and is also the industry standard for the identification of sheet metals properties.

The motivation of this paper is to improve the accuracy of FE stamping analysis with isotopic hardening plasticity modeling based on material stress–strain data on the basis of simple tension tests. For this purpose, mechanical properties of a dual-phase steel are determined with uniaxial tensile loadings. Standard uniaxial tests are conducted to determine elastic modulus, flow curves and plastic ratios of DP600 steel of 0.8 mm thickness at room temperature. Moreover, tensile loadings with repeated unloading–reloading cycles are performed to determine Young's modulus evolution during uniaxial plastic deformation. Anisotropy of DP600 steel is described with Hill's orthotropic yield function, and strain-hardening behavior is simulated with isotopic hardening plasticity model. Then, stamping process simulations of an automotive structural part are performed. FE results calculated with both models are evaluated in terms of plastic strain, thickness and springback distributions. Predicted part geometries are also compared with surface scanning of manufactured parts.

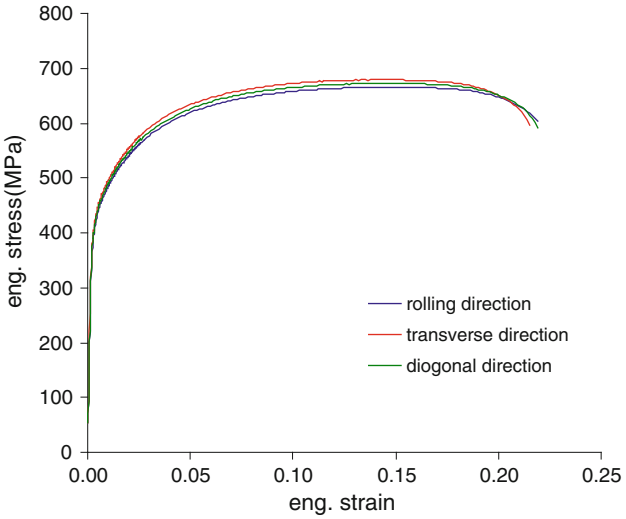

Fig. 1 Engineering stress–strain curves of 0.80 mm thickness DP600 steel

2 Material Testing

Mechanical properties of DP600 steel were obtained with tensile tests conducted according to ASTM E8 standard [15]. Specimens having a width of 12.5 mm and a gauge length of 50.0 mm were prepared from rolling, transverse and diagonal directions of 0.80 mm thickness sheets. All tensile tests were conducted using a Zwick tensile testing machine. During uniaxial tensile loadings, elongations were measured using an automatic contacting extensometer, and transverse displacements in specimen width direction were also obtained by means of a transverse averaging extensometer. Figure 1 shows engineering material stress–strain curves determined from standard tensile tests.

The true strain components in longitudinal and width directions were also determined from extensometer strains, and volume constancy is assumed in calculating true thickness strains in rolling, transverse and diagonal directions. Only the part of experimental curves up to uniform elongation was included in true stress and plastic strain calculations, and flow curves in all directions are used to determine material strength coefficient K and strain-hardening exponent n. Plastic strain ratios in rolling, diagonal and transverse directions (r_0, r_{45}, r_{90}) were calculated using thickness and width strain values corresponding to an elongation of 14 %

Table 1 The mechanical properties of DP600 steel

Test direction	Elastic modulus (GPa)	Yield stress (MPa)	K (MPa)	n	r-ratio
Rolling	201.5	365.4	1,090.9	0.154	0.855
Diagonal	202.3	372.9	1,096.7	0.153	0.887
Transverse	204.7	379.2	1,113.5	0.151	0.994

that was approximately 1–2 % less than maximum uniform elongations in three directions [16]. Young's moduli in three material directions were also determined by line-fitting to the linear part of true stress–true strain curves and the calculated moduli are employed to determine initial yield stress of DP600 steel by 0.2 % strain offset method [15]. Table 1 summarizes mechanical properties and parameters related to flow properties of DP600 steel of thickness 0.80 mm calculated with tensile test data. An inspection of r values from rolling, diagonal and transverse directions indicates a directional variation with respect to rolling axis and proves the use of an anisotropic yield function in sheet metal deformation analysis [17].

In addition to monotonic tensile loadings, tensile tests with repeated unloading–reloading cycles were performed to assess the stiffness degradation during plastic deformation. A single specimen is subjected to repeated tensile cycles between maximum stress and zero stress for a predetermined set of engineering strain values. Figure 2 shows the stress and strain variation along the rolling direction for seven loading–unloading–reloading cycles. A comparison of stress–strain curves obtained from monotonic tensile loadings and tensile loadings with intermittent unloading to zero stress level indicates that the material deformation response follows the monotonic curve after reloading and can be described with true stress–true strain curve along the same material direction. Moreover, a nonlinear hysteresis in material stress–strain response is constantly observed during unloading–reloading stage for all prestrain levels. In each hysteresis loop, an upper intersection point A is observed to be slightly lower than the maximum stress level in material flow curve at the same prestrain level (Fig. 2b).

In this study, the hysteresis characteristic of experimental stress–strain histories during unloading–reloading cycles is employed as a practical definition of Young's modulus as function of prestrain. Accordingly, the slope of line segment AB connecting the zero-stress level, point B, to the intersection point A is defined as the prestrained elastic modulus of DP600 steel. This modeling approach is consistent with the application of phenomenological metal plasticity based on the yield surface concept in stress space and replaces the nonlinear hysteresis loop with a straight line segment up to material stress–strain curve. The resulting variation

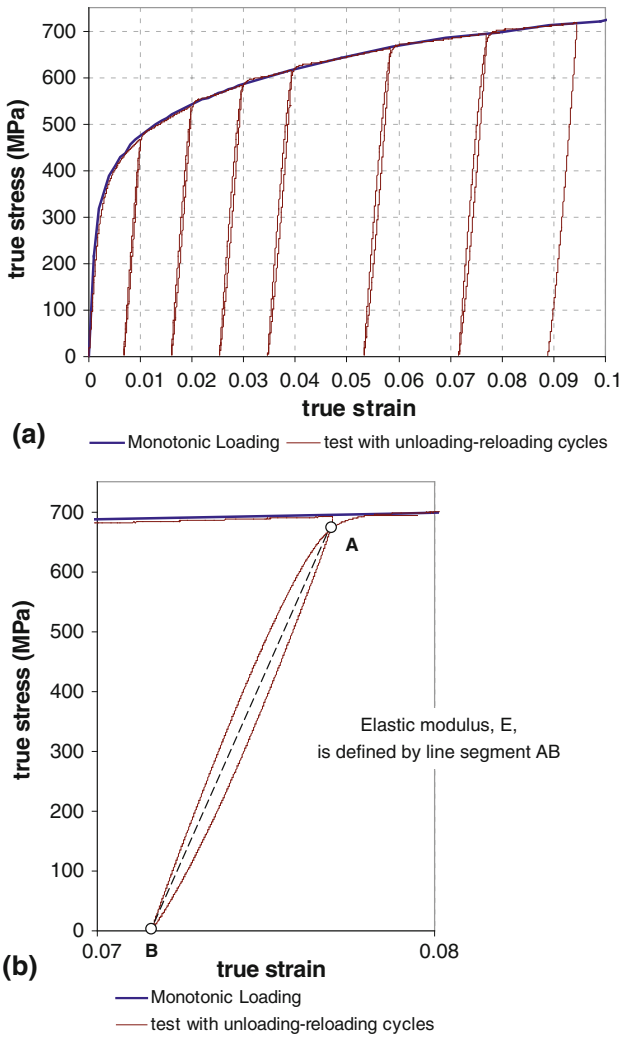

Fig. 2 **a** True stress–true strain curves from tensile test and tensile test with repeated unloading–reloading cycles along rolling direction. **b** Hysteresis loop observed with unloading at near 8 % prestrain and line segment defining Young's modulus E

of elastic modulus as a function of plastic strain is shown graphically in Fig. 3 together with the corresponding analytical curve fitted on the basis of the following exponential function.

$$E = E_0 - (E_0 - E_s)(1 - e^{-\zeta \varepsilon_p}) \quad (1)$$

In above equation, E_0 and E_s are initial Young's modulus and its limiting value with increasing plastic strain ε_p. Fit parameter ζ denotes the saturation rate. Table 2 lists the computed constants from curve-fitting calculations based on the aforementioned identification technique applied to the experimental points along rolling, diagonal and transverse directions. A comparison of the elastic moduli variations with plastic deformation indicates slight differences in terms of saturation rates and limiting values, but nearly a 30 GPa decrease in Young's moduli was also noted irrespective of material

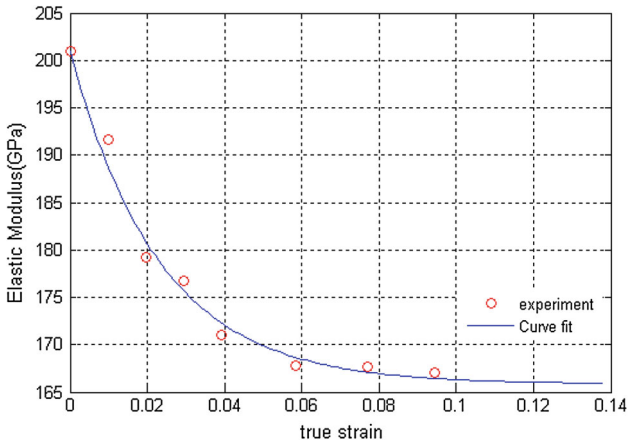

Fig. 3 The variation of elastic modulus of DP600 steel with plastic deformation

Table 2 Elastic moduli variations of DP600 steel

Test direction	E_0 (GPa)	E_s(GPa)	ζ
Rolling	201.5	166.0	43.4
Diagonal	202.3	169.1	39.7
Transverse	204.7	172.5	41.3

testing direction. This corresponds to a stiffness degradation of approximately 17.5 % along the rolling direction.

3 Plasticity Modeling of DP600 Steel

Sheet metal deformation models in industrial FE stamping applications are commonly based on phenomenological plasticity models that are intended to simulate multi-axial material deformations at macroscopic scale [8–14]. In these models, preferred orientation of polycrystalline grains due to rolling processes is the major source of directional dependence of sheet metal flow stress [17]. Furthermore, plastic anisotropy is described by means of a yield function defining the initial yield loci in the stress space and the evolution of the yield condition during plastic deformation is defined using a hardening rule [9,11,13]. In this study, sheet deformations are described with Hill's quadratic yield function f given by the following expression [17],

$$f = \left\{(G+H)\sigma_x^2 - 2H\sigma_x\,\sigma_y + (F+H)\sigma_y^2 + 2N\sigma_{xy}^2\right\}^{\frac{1}{2}} - \sigma_0 \tag{2}$$

where G, H, F and N are Hill's orthotropic parameters. σ_x, σ_y and σ_{xy} represent in-plane Cauchy stress components and σ_0 is the equivalent stress. Isotropic hardening will be assumed so that the yield surface retains its initial shape and orientation in stress space throughout deformation. Moreover, the plastic anisotropy is simulated with the uniform expansion of yield surface, and an accumulated equivalent plastic strain $\bar{\varepsilon}_p$ is introduced as an internal state variable to calculate the yield surface size $\sigma_0(\bar{\varepsilon}_p)$ in stress space.

$$f = \left\{(G+H)\sigma_x^2 - 2H\sigma_x\sigma_y + (F+H)\sigma_y^2 + 2N\sigma_{xy}^2\right\}^{\frac{1}{2}} - \sigma_0(\bar{\varepsilon}_p) \tag{3}$$

Taking rolling, diagonal and transverse directions of the sheet metal as reference orthotropic axes of Hill's yield function, effective stress and accumulated equivalent plastic strain curve will be equal to true stress–true plastic strain curve determined in tensile test along rolling direction. Furthermore, Hill's orthotropic parameters are determined by means of plastic anisotropy coefficients in rolling, diagonal and transverse directions (r_0, r_{45}, r_{90}) and will be calculated with the following expressions.

$$G = \frac{1}{1+r_0} \tag{4}$$

$$H = \frac{r_0}{1+r_0} \tag{5}$$

$$F = \frac{r_0}{r_{90}(1+r_0)} \tag{6}$$

$$N = \frac{(r_0+r_{90})(2r_{45}+1)}{2r_{90}(1+r_0)} \tag{7}$$

Figure 4 shows graphically the initial yield locus of DP600 steel computed under biaxial stress condition. Since isotopic hardening is assumed, the yield surface will expand uniformly in stress space and effective stress–equivalent plastic strain curve determines the evolution of yield loci during deformation process.

4 Stamping Analysis of a DP600 Steel Roof-stiffener Part

The effect of Young's modulus evolution on the accuracy of FE springback predictions is evaluated with process simulations of an automotive roof-stiffener structure made of the same DP steel grade investigated in previous section (Fig. 5). FE simulations on the basis of presented plasticity modeling approach were performed using commercially available Ls-Dyna program [18], and part shape distortions were predicted during die face development of the stamping tooling. Stamping simulations are performed in two sequential steps using two different FE models [9]. In the first step, a forming FE model is prepared using die surfaces and blank geometry, and sheet metal deformations are calculated using an explicit dynamic analysis. This FE analysis provides part geometry together with thickness, stress and strain distributions at the

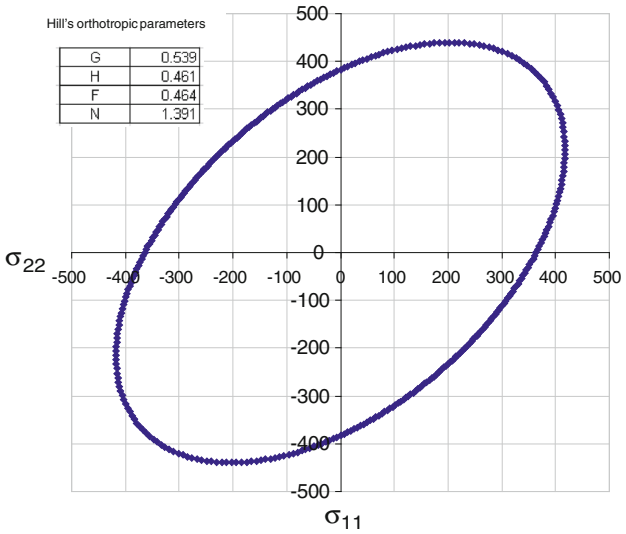

Fig. 4 The yield loci of DP600 steel in principal stress space (all values are in MPa)

Fig. 5 A DP600 steel roof-stiffener part

end of forming process while tooling surfaces are still in contact with the deformed blank. Next, a springback analysis follows to determine roof-stiffener geometry after the release of the contact with stamping die. This springback step is conducted by an implicit, geometrically nonlinear, static analysis in which only blank FE meshes together with thickness, stress and strain distributions at the end of the forming step constituting the main modules of the computational model.

Since roof-stiffener geometry is symmetric about its transverse direction, only halves of the blank and tooling surfaces were included in forming analyses. Figure 6 shows the FE model and the section plane on which symmetry boundary conditions were applied in both forming and springback steps. In forming model, tool surfaces were meshed with triangular and rectangular rigid facet elements and a minimum of six elements were used to have a smooth and accurate representation of geometric features such as die radii and surface transitions. In FE meshing of DP600 steel blank, fully integrated four-node shell elements with 9 through-thickness integration points were used with a uniform element size of 1 mm (Fig. 6). A constant coefficient of friction, 0.125, is used for the contact interface between blank and rigid stamping tooling. In order to determine the coefficient of friction required in FE modeling the forming process, draw-bead simulator tests were conducted using sheet metal strips of size 50 mm × 200 mm [19]. Since no lubrication is applied in roof-stiffener stamping process, all friction tests were also conducted under dry friction conditions, and a constant drawing speed of 30 mm/s was employed during drawing over bead and contra-bead rollers of radius 5 mm. The arithmetic average of five friction coefficients determined using experimental force data was used as modeling parameter in all simulations. In forming analyses, first a constant blankholder force of 90 tons was applied on blankholder, and then stiffener-part is stamped under the action of a 66 mm die stroke. Next, FE mesh of the deformed blank is submitted to springback analysis retaining symmetry boundary conditions, and final part geometry and thickness distributions were obtained using an implicit static FE computation. In order to remove three rigid-body modes of deformed blank (two translations in Y and Z directions, and a rotation about X direction), three nodes are additionally constrained in X, Y and Z directions properly in springback analysis model (Fig. 6). Two of these nodes were located on the middle of the blank along the symmetry line and the other node is chosen very close to these two nodes. Consequently, the blank is free to spring back in both transverse and longitudinal directions while a small zone of size approximately 2 mm × 2 mm

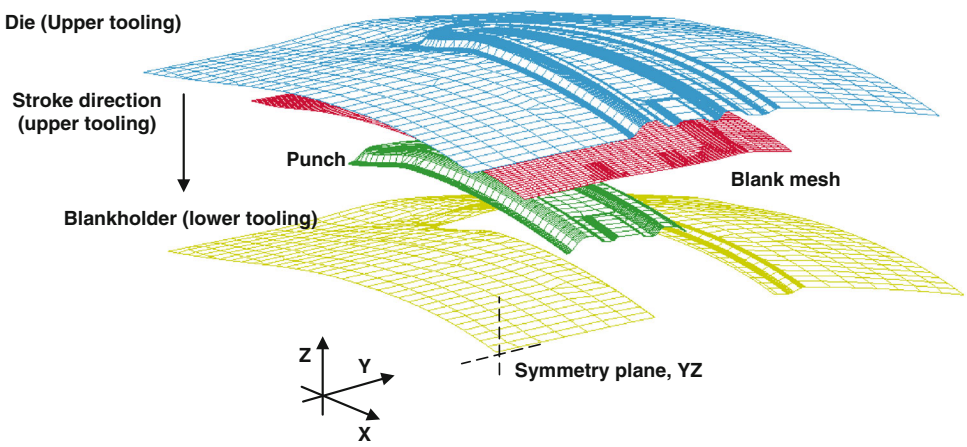

Fig. 6 FE forming analysis model of roof-stiffener part

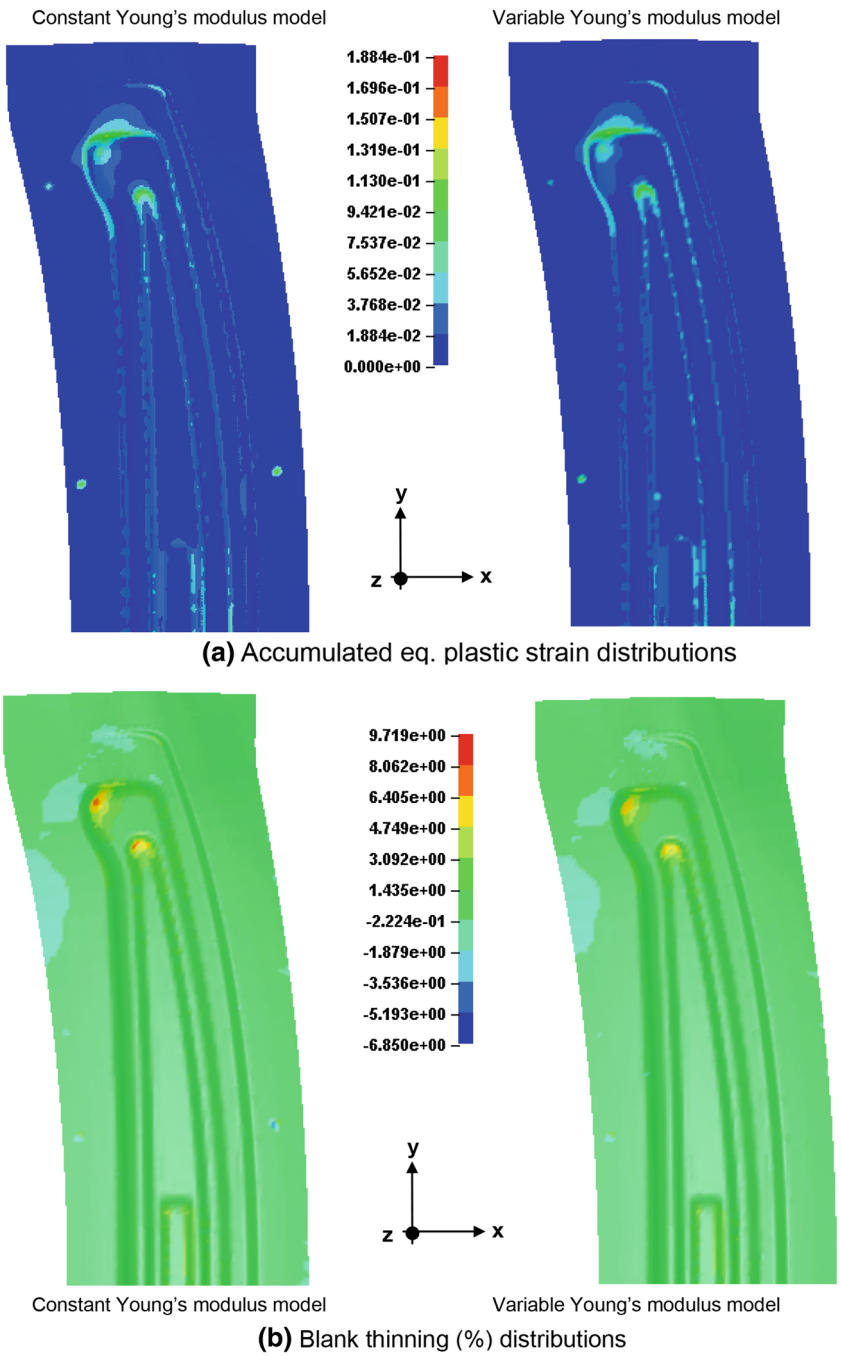

Fig. 7 Computed effective plastic strain and blank thinning distributions of roof-stiffener part

at the center of the blank is fixed. The outlined FE modeling approach is followed in all stamping simulations using identical FE meshes, boundary conditions and contact parameters. The plasticity model parameters are the same for all FE models, and Young's modulus variation is included in FE models using the exponential function whose parameters are taken from the curve-fit along the rolling direction. It is also worth to state that FE models that were briefly presented here were developed on the basis of a preliminary mesh convergence study to ensure the consistency of computational results.

4.1 Results and Discussion

Stamping process simulations were performed using the presented two-step analysis approach, and roof-stiffener geometry, part thickness and plastic strain distributions were calculated using Hill's anisotropic plasticity models with both constant and variable Young's moduli. The same FE meshes, boundary conditions and computational settings were employed in all FE simulations performed using Ls-Dyna solver on 8-processors Windows XP64 machine. A comparison of

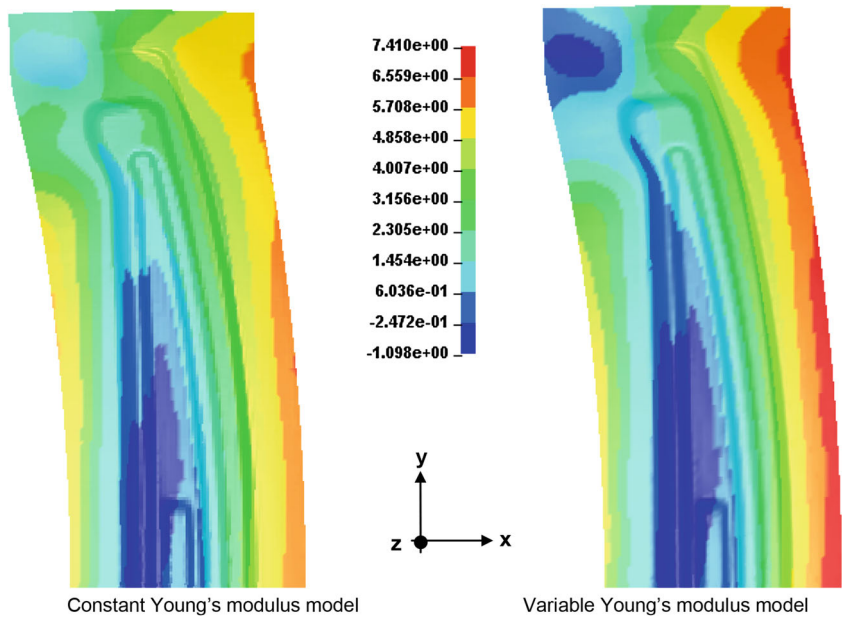

Fig. 8 Computed springback distributions of roof-stiffener part

calculated effective plastic strain and blank thickness values indicates that both models produced fairly similar distributions and most critical material points were determined to be at the same location (Fig. 7). The maximum differences between two predictions are approximately 4–6 % in terms of effective plastic strain and blank thinning values, and the results with variable elastic modulus FE model are lower than those calculated with constant modulus case. A similar conclusion can be drawn for the direction of springback computed with both models, and part distortions on the overall have a tendency to reduce the major curvature of roof-stiffener about its symmetry axis (Fig. 8). In addition, in FE analyses with both models, maximum springback deformation was occurred at the mid-section of stiffener part, as also determined in stamping experiments. Thus predicted shape distortion patterns were qualitatively in agreement with actual observations in stamped parts.

There were, however, considerable differences between magnitudes of springback predicted with both FE models. Figure 8 shows calculated displacement distributions along Z axis and compares shape deviations of stamping part with respect to part forming geometries computed with constant and variable moduli FE models. The maximum springback displacement computed with variable modulus model is 7.4 mm at the mid-section of roof-stiffener while constant modulus model predicted 5.2 mm maximum springback almost at the same section (Fig. 8). Since both FE results were obtained with Hill's isotopic hardening plasticity model using identical computational settings, differences between two springback predictions are caused by differences in calculated strain recovery during springback step. Since the recovery strain $\Delta\varepsilon^{\text{springback}}$ at any material point is determined by both the magnitude of stress change during springback and the instantaneous value of Young's modulus, it is essential to investigate the changes in stress distributions before and after springback step. Figure 9a shows bending stress distributions along the section cut at part symmetry plane before and after springback steps. An exploration of section stresses shows that both FE models have a nearly identical $\sigma_{\text{for min g}}$ and $\sigma_{\text{springback}}$ variations before and after springback. Consequently, the differences between FE springback predictions are mainly caused by the different strain recoveries computed for the same material point. Accounting the elastic moduli variation in material plasticity modeling increases the magnitude of recovery strain computed in springback analysis.

In order to assess the accuracy of part geometries calculated with both FE models, top surfaces of five stamped roof-stiffener parts were scanned using an optical measurement system. Measurement samples were chosen randomly among manufactured parts that were produced following a warm-up period of stamping die. Part surfaces were scanned at one measurement session, and collected sets of measurement points were averaged arithmetically to generate a representative surface mesh composed of triangular facets for comparison purposes. Figure 9b shows FE predicted section profiles that were used for bending stress distributions and measurement data from surface scanning of stamped parts. An examination of profile plots indicates that both model predictions conform partially to measured profile, but underestimate actual shape distortions determined in manufactured parts. Calculations with variable modulus have, nevertheless, reduced maximum geometry deviation approximately by 20 % and constantly improved shape correlation. The

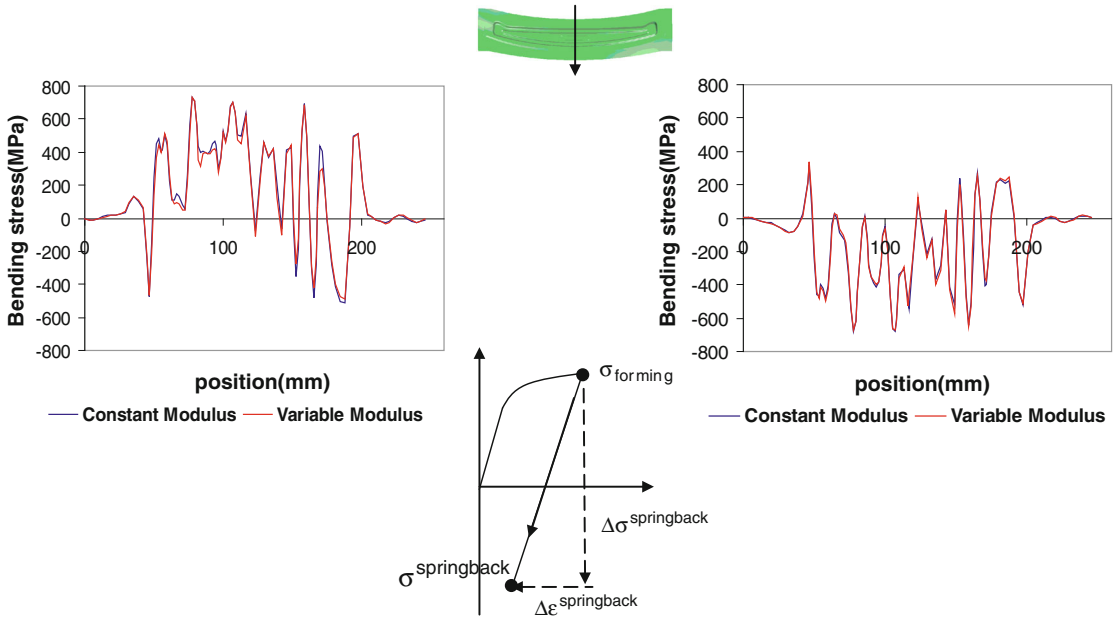

(a) Bending stresses along the part mid-section: (left) forming step, (right) after springback

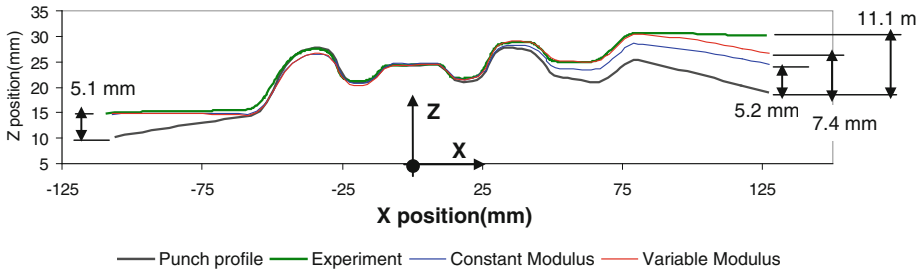

(b) Part Profiles at mid-section: FE-predictions and surface scanning experiment

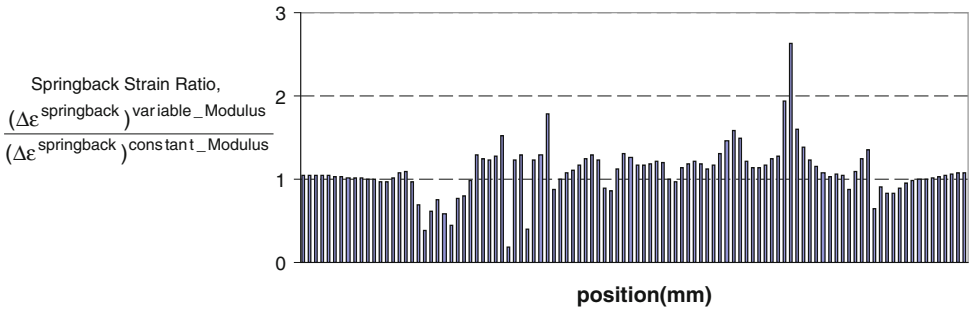

(c) Ratio of springback strains predicted with variable and const. moduli cases.

Fig. 9 The effect of elasticity evolution on the bending strain distribution during loading and unloading steps

effect of magnitude of elastic recovery on the calculated section profiles is also assessed by taking the ratio of recovery strains computed with variable modulus model to that from constant modulus FE model. A calculation of strain ratio along the mid-section profile results in a variation generally located above unity line (Fig. 9c), and as the strain ratio increases, the part profile predicted with variable modulus model deviates from that of constant modulus case. This situation proves the elastic modulus evolution during stamping process, similar to that in tensile tests with unloading–reloading cycles. Furthermore, the accuracy of FE springback predictions has been improved considerably by accounting

Young's modulus reduction determined on the basis of proposed uniaxial testing approach.

5 Conclusion

In this study, the effect of Young's modulus evolution on the accuracy of FE springback predictions was investigated by stamping simulations of a DP steel automotive part and comparisons with experiments. All plasticity modeling parameters were determined with standard tensile tests, and for simplicity, isotopic hardening is chosen in the Hill's plasticity modeling. Young's modulus variation was determined on the basis of uniaxial tensile tests with repeated unloading–reloading cycles. A minimum 30 GPa reduction in material elastic modulus was observed in all tests and this indicates approximately 17.5 % stiffness degradation in rolling direction. Then FE stamping analyses of a roof-stiffener part were conducted using presented plasticity modeling with both constant and variable Young's moduli. Effective plastic strain and part thickness distributions calculated with both models were fairly similar and maximum differences were determined to be 4 and 6 %, respectively. A similar situation holds for predicted springback distributions, but springback magnitudes calculated with variable modulus model were constantly higher. Computed geometries with both FE models were, furthermore, evaluated with surface scanning of manufactured parts. While stamping geometries predicted with both models underestimate actual shape distortions determined in manufactured parts, calculations with variable modulus have reduced maximum geometric deviation by 20 % and constantly improved shape correlation. An evaluation of FE results proved the key role of elastic recovery strain in the prediction of final part geometry and revealed the significance of stiffness degradation during stamping process.

Acknowledgments This study was performed as a part of the research project supported by Coskunoz Holding and Turkish Scientific and Technological Research Council (TUBITAK). Author thanks to Aydin Kuntay of Bias Engineering for providing the technical material and supporting the use of the LS-Dyna in this study. Also helps of technical staff of Coskunoz-Metalform are gratefully acknowledged.

References

1. Vehicle Crashworthiness and Occupant Protection. Auto/Steel Partnership & American Iron and Steel Institute, Southfield (2004)
2. Lightweight Rear Chassis Project Report. Auto/Steel Partnership & American Iron and Steel Institute, Southfield (2008)
3. Mowrtage, W.: Low-rise 3D panel structures for hot regions: design guidelines and case studies. Arab. J. Sci. Eng. **37**(3), 587–600 (2012)
4. Murali, G.; Gopal, M.; Rajadurai, A.: Effect of circular and rectangular drawbeads in hemispherical cup forming: finite element analysis and experimental validation. Arab. J. Sci. Eng. **37**(6), 1701–1709 (2012)
5. Sadagopan, S.; Urban, D.: Formability characterization of a new generation high strength steels. American Iron and Steel Institute, Pittsburgh (2003)
6. Roll, K.; Weigand, K.: Tendencies and new requirements in the simulation of sheet metal forming processes. Comput. Methods Mater. Sci. **9**, 12–24 (2009)
7. Automotive Steel Design Manual. Auto/Steel Partnership & American Iron and Steel Institute, Southfield (2002)
8. Haddadi, H.; Bouvier, S.; Levée, P.: Identification of a microstructural model for steels subjected to large tensile and/or simple shear deformations. J. Phys. **IV**(11), 329–337 (2001)
9. Chun, B.K.; Jinn, J.T.; Lee, J.K.: Modeling the Bauschinger effect for sheet metals, part I: theory. Int. J. Plast. **18**, 571–595 (2002)
10. Sung, J.H.; Kim, J.N.; Wagoner, R.H.: A plastic constitutive equation incorporating strain, strain-rate, and temperature. Int. J. Plast. **26**(12), 1746–1771 (2010)
11. Firat, M.: U-channel forming analysis with an emphasis on springback deformation. Mater. Des. **28**, 147–154 (2007)
12. Wagoner, R.H.; Li, M.: Simulation of springback: through-thickness integration. Int. J. Plast. **23**(3), 345–360 (2007)
13. Yoshida, F.; Uemori, T.: A model of large-strain cyclic plasticity describing the Bauschinger effect and work hardening stagnation. Int. J. Plast. **18**, 661–686 (2002)
14. Haddadi, H.; Bouvier, S.; Banu, M.; Maier, C.; Teodosiu, C.: Towards an accurate description of the anisotropic behaviour of sheet metals under large plastic deformations: modelling, numerical analysis and identification. Int. J. Plast. **22**, 2226–2271 (2006)
15. ASTM Standard E8-01. Standard Test Methods for Tension Testing of Metallic Materials. ASTM International, West Conshohocken (2001)
16. ASTM Standard E517. Standard Test Method for Plastic Strain Ratio r for Sheet Metal. ASTM International, West Conshohocken (2010)
17. Banabic, D.; Bunge, H.J.; Pohlandt, K.; Tekkaya, A.E.: Formability of Metallic Materials, Springer, Berlin (2000)
18. Hallquist, J.O.: Ls-Dyna Theory Manual. LSTC, Livermore (2006)
19. Nine, H.D.: The applicability of Coulomb's friction law to drawbeads in sheetmetal forming. J. Appl. Metal Work. **2**(3), 200–210 (1982)